

AperTO - Archivio Istituzionale Open Access dell'Università di Torino

**Monitoring the time-averaged discharge rates, volumes and emplacement style of large lava flows by using MIROVA system: the case of the 2014-2015 eruption at Holuhraun (Iceland)**

**This is the author's manuscript**

*Original Citation:*

*Availability:*

This version is available <http://hdl.handle.net/2318/1701175> since 2019-05-08T11:46:03Z

*Published version:*

DOI:10.4401/ag-7749

*Terms of use:*

Open Access

Anyone can freely access the full text of works made available as "Open Access". Works made available under a Creative Commons license can be used according to the terms and conditions of said license. Use of all other works requires consent of the right holder (author or publisher) if not exempted from copyright protection by the applicable law.

(Article begins on next page)



ACCEPTED ON ANNALS OF GEOPHYSICS, 61, 2018; Doi:  
10.4401/ag-7749

## Monitoring the time-averaged discharge rates, volumes and emplacement style of large lava flows by using MIROVA system: the case of the 2014-2015 eruption at Holuhraun (Iceland)

D. Coppola<sup>(1)(2)</sup>, S. Barsotti<sup>(3)</sup>, C. Cigolini<sup>(1)(2)</sup>, G., M. Laiolo<sup>(1)(4)</sup>, M.A.,  
Pfeffer<sup>(3)</sup>, M. Ripepe<sup>(4)</sup>

(1) Dipartimento di Scienze della Terra, Università di Torino, Via Valperga Caluso  
35, 10125 Turin, Italy

(2) NatRisk, Centro Interdipartimentale sui Rischi Naturali in Ambiente Montano e  
Collinare, Università degli Studi di Torino, Italy

(3) Icelandic Meteorological Office. Bustaðavegi 7-9, 108 Reykjavik, Iceland

(4) Dipartimento di Scienze della Terra – Università di Firenze. Via G. La Pira 4,  
50121 Florence, Italy.

1 **Monitoring the time-averaged discharge rates, volumes and emplacement style**  
2 **of large lava flows by using MIROVA system: the case of the 2014-2015 eruption**  
3 **at Holuhraun (Iceland)**

4

5 *D. Coppola<sup>(1)(2)</sup>, S. Barsotti<sup>(3)</sup>, C. Cigolini<sup>(1)(2)</sup>, G., M. Laiolo<sup>(1)(4)</sup>, M.A., Pfeffer<sup>(3)</sup>, M. Ripepe<sup>(4)</sup>*

6

7 **Corresponding author:** Coppola Diego ([diego.coppola@unito.it](mailto:diego.coppola@unito.it)).

8

9 *(1) Dipartimento di Scienze della Terra, Università di Torino, Via Valperga Caluso 35, 10125*  
10 *Turin, Italy*

11 *(2) NatRisk, Centro Interdipartimentale sui Rischi Naturali in Ambiente Montano e Collinare,*  
12 *Università degli Studi di Torino, Italy*

13 *(3) Icelandic Meteorological Office. Bústaðavegi 7- 9, 108 Reykjavík, Iceland*

14 *(4) Dipartimento di Scienze della Terra – Università di Firenze. Via G. La Pira 4, 50121*  
15 *Florence, Italy.*

16

17

18

19

20

21

22

23

24

25 **Abstract**

26 The 2014-2015 eruption at Holuhraun has produced more than 1.5 km<sup>3</sup> of basaltic magma and can be  
27 considered one of the major effusive events of the last two centuries in the world. During this eruption  
28 the MIROVA system (a volcanic hot-spot detection system based on MODIS middle infrared – MIR  
29 - data) has been used to detect and locate the active portions of the lava flow(s), and to measure the  
30 heat radiated by the growing lava field. According to these data the eruption was characterized by a  
31 slow decay of the radiant power, accompanied by a change in the lava transport mechanism that  
32 shifted from open channels, at the beginning of the eruption, to lava tubes, during the last months of  
33 activity. Despite the evident evolution of lava transport mechanism, we found that the overall  
34 decreasing trend of the thermal flux was mainly controlled by the exponential decline of lava  
35 discharge rates, while the increasing insulation of the flow field had a strong impact in transporting  
36 efficiently the lava at the distal flow front(s). Our results suggest the apparent time averaged lava  
37 discharge rates (*TADR*), derived from satellite thermal data, may fluctuate around the real effusion  
38 rate at the vent, especially in the case of large lava flows emplacing in nearly flat conditions. The  
39 magnitude and frequency of these fluctuations are mainly controlled by the emplacement dynamic,  
40 (i.e. occurrence of distinct major flow units), while the transition from channel- to tube-fed lava  
41 transport mechanism play only a minor role ( $\pm 30\%$ ) in the retrieval of *TADR* using MIR data . When  
42 the *TADR* values are integrated to calculate erupted lava volumes, the effects of pulsating  
43 emplacement dynamic become smoothed and the eruptive trend become more clear.

44 We suggest that during the Holuhraun's eruption, as well as during many other effusive eruptions,  
45 the MIR-derived radiant flux essentially mimic the overall trend of lava discharge rates, with only a  
46 minor influence due to the emplacement style and evolving eruptive conditions. From a monitoring  
47 and operational perspective, MIROVA demonstrates to be a very valuable tool to follow and,  
48 possibly, forecast the evolution of on-going effusive eruptions.

49

## 1. Introduction

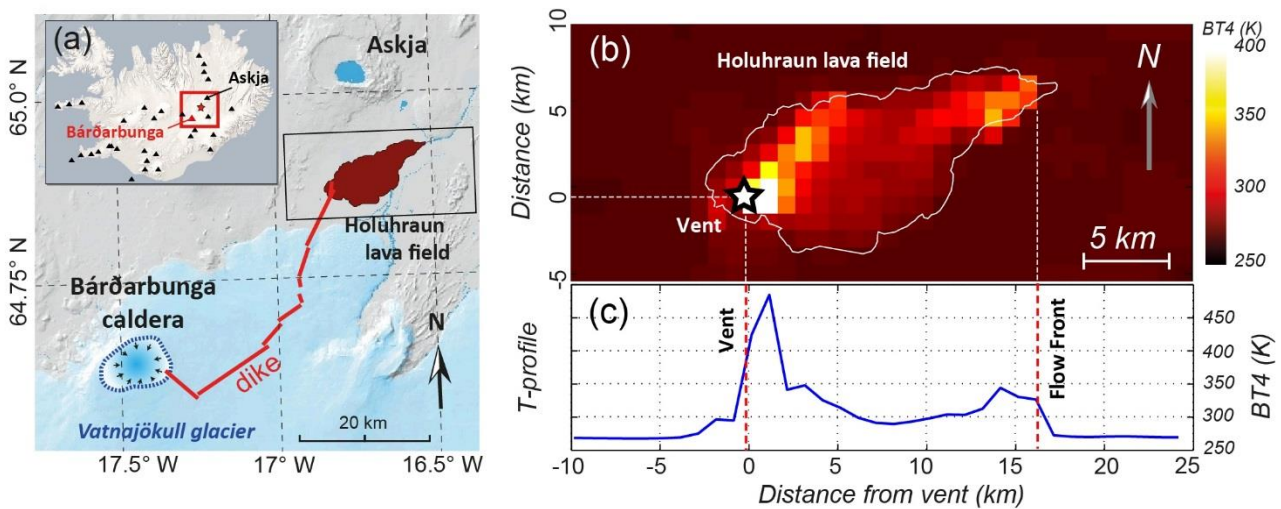
On August 29<sup>th</sup> 2014, one of the largest effusive eruption of the last 3 centuries took place along the Eastern Volcanic Zone (EVZ) of Iceland, about 45 km north-east of Bárðarbunga volcanic system (Gudmunsson, et al., 2014). The new eruption followed 15 days of sustained seismicity and accompanied the propagation of a 45 km long dike (Sigmundsson et al., 2015) that unlocked an historical eruptive path named Holuhraun (Sigurðsson and Sparks, 1978). The emission of lava persisted at very high rate for 180 days up to February 27<sup>th</sup>, 2015 when the activity was declared over (Gislason et al., 2015). The eruption was characterized by a slow decay of effusion rate (Coppola et al., 2017) that accompanied a coeval slow subsidence of the Bárðarbunga caldera (Gudmundsson et al., 2016). The clear link between the two processes provided evidences of an inelastic eruption whereby the lateral magma withdrawal was essentially linked to the gravity-driven collapse of the summit caldera (Coppola et al., 2017, Gudmundsson et al. 2016). About 84 km<sup>2</sup> of nearly flat land was covered by the new lava field that reached a maximum extend of about 18 x 5 km (Figure 1) and thickness up to 40 m (Gislason et al., 2015, Pedersen et al. 2017).

The prohibitive environmental conditions that might characterize these latitudes made field observations at the eruptive site very hard, especially on a continuous basis and for several months during the winter time. In these conditions, space-based thermal data have been extremely useful since they allowed a safe detection, location and quantification of the radiant flux produced by the effusive activity. In particular, infrared data acquired by MODIS (Moderate Resolution Imaging Spectroradiometer) and elaborated through the MIROVA volcanic hotspot detection system, (Coppola et al., 2016; [www.mirovaweb.it](http://www.mirovaweb.it)), were delivered to the Icelandic Meteorological Office (IMO) as part of its daily operational monitoring activity of the Holuhraun eruption.

Since the beginning of the eruption the main tasks of satellite thermal data were: (i) to provide information about the location of active lava flow areas and front, (ii) to give an estimation of lava discharge rates and erupted volumes and finally (iii) to identify the ongoing effusive trend (steady,

75 waning or waxing). The latest two points became a priority after a couple of months when the winter  
 76 season and the low-light conditions made the eruptive site hardly accessible and field observations  
 77 became more and more rare and difficult. The calculation of effusion rates from satellite thermal data  
 78 (the so called “thermal proxy”), become one of the main topic discussion among a thermal remote  
 79 sensing group, established in that occasion by Dr. Thor Thordarson (Harris et al., 2016a). One of the  
 80 main questions discussed within the group was “whether the subtle, but persistent decay of thermal  
 81 flux indicated by satellite measurements, was caused by a real, slow decline of the effusion rate or  
 82 reflected the increasing insulation of the growing lava field and the development of a lava tube system  
 83 (Pedersen et al., 2017)

84



85

86 **Figure 1.** (a) Location of the Bárðarbunga-Holuhraun volcanic system showing the ice covered, 10-km-wide caldera of  
 87 Bárðarbunga and the 2014-2015 lava field at Holuhraun. (b) Example of MODIS-derived thermal image (spatial  
 88 resolution of 1 km) showing the Brightness Temperature at 4 μm (BT4) recorded on February 03<sup>rd</sup>, 2015 over the  
 89 Holuhraun lava field (white line). The star indicates the approximate location of the vent. (c) Temperature profile along  
 90 W-E direction, obtained by calculating the maximum BT4 along each vertical (N-S) line. The position of the flow front  
 91 is marked by the easternmost thermally anomalous pixel (see the text for details).

92

93

94

95 In this paper we present time-averaged lava discharge rates and volumes, derived by using MIROVA  
96 system, and we compare the results with field and independent measurements collected during and  
97 after the Holuhraun eruption. The comparison reveals the role of changing emplacement style in the  
98 lava discharge rates calculation and outlines the contribution of MIROVA in safely tracking this large  
99 effusive eruptions from space.

100

## 101 **2. Time-averaged discharge rates from satellite thermal data: background and open** 102 **questions**

103 The relationship between effusion rates and thermal emissions of lava flows has received increasingly  
104 attention during the past three decades (a full list of 46 papers published between 1990 and 2005 is  
105 reported in [Harris 2013](#)). The methods, limits and applications of this approach are part of a book  
106 expressly focussed on detecting, modelling and responding to effusive eruptions ([Harris et al., 2016b](#)),  
107 whereas exhaustive overview of the physic behind mass and energy flow through a lava flow system  
108 is provided by a series topical works ([Pieri and Baloga 1986](#), [Crisp and Baloga 1990](#), [Harris et al.,](#)  
109 [1997](#), [Wright et al., 2001](#), [Harris et al., 2007](#), [Harris and Baloga 2009](#); [Dragoni and Tallarico 2009](#),  
110 [Coppola et al, 2013](#); [Garel et al., 2012, 2014, 2015](#), [Tarquini \(2017\)](#), among others). Here, we outline  
111 the basic principles of this technique and we summarize the open questions that have been addressed  
112 in this work.

113 To describe volumetric flow rates of erupted lavas, we use the terminology given by [Harris et al.](#)  
114 [\(2007\)](#). We use the generic term *effusion rate*, to describe the instantaneous rate at which lava is  
115 erupted from the vent at any time. The term *mean output rate (MOR)* is used to describe the final  
116 volume of erupted lava divided by the total duration of the eruption. Finally, we used the term *time-*  
117 *averaged lava discharge rate (TADR)* to describe the volume of lava emplaced during a specific time  
118 interval ([Harris et al., 2007](#)). This definition better applies to the use of satellite-based methods, for

119 measuring the changes in lava volume over a given period of time prior the image acquisition (Wright  
120 et al., 2001).

121 Currently, two main methods exist to estimate *TADR*s from space-based thermal data; the method of  
122 Harris et al. (1997), simplified later by Wright et al. (2001), and the method of Coppola et al., (2013).

123 Both the methods rely on the original heat balance approach (Pieri and Baloga, 1986), stating that the  
124 *mean output rate MOR* ( $\text{m}^3 \text{s}^{-1}$ ) of a cooling-limited lava flow, is related to its final plan area  $A$   
125 (attained when the flow achieves its final length,  $L$ ), by:

126

$$127 \quad MOR = \frac{\varepsilon \sigma T_e^4}{\rho C_p (T_0 - T_{stop})} A(L) \quad (\text{eq. 1})$$

128

129 where  $\rho$  ( $\text{kg m}^{-3}$ ) and  $C_p$  ( $\text{J kg}^{-1} \text{K}^{-1}$ ) are the bulk density and heat specific capacity of lava,  
130 respectively,  $T_e$  (K) is the effective radiation temperature of the flow,  $T_0$  (K) is the lava eruption  
131 temperature, and  $T_{stop}$  (K) is the temperature of the flow front at the time the flow has cooled to a halt.

132 In this framework, the effective radiation temperature is defined as “the temperature at which the flow  
133 would radiate if it had a constant surface temperature throughout the emplacement of the flow” (Crisp  
134 and Baloga, 1990).

135 Harris et al., (1997), applied this approach to satellite thermal data, developing what is actually called  
136 the “thermal proxy”. Further works (Wright et al., 2001; Harris et al. 2007, 2009) refined and  
137 simplified this method suggesting that the equation 1, when applied to satellite radiance data, provides  
138 discharge rates that are not necessarily averaged over the total duration of an eruption, but rather over  
139 “some time” prior to the satellite acquisition. Here, the effective radiation temperature,  $T_e$ , takes a  
140 specific meaning, since it represents the average surface temperature over “some time” prior to the  
141 satellite acquisition, weighted according to the radiative heat flux (Harris and Baloga, 2009).  
142 Accordingly, Harris et al., (2007) proposed to use the term “*time-averaged discharge rate*” (*TADR*),  
143 in order to describe the discrete measurements of lava flux retrieved from single satellite thermal



144 images. [Wright et al., \(2001\)](#) also argued that all values except *MOR* (or *TADR*) and *A* are assumed  
145 a priori in equation 1 so that the thermal proxy reduces to a simple relationship whereby:

146

$$147 \quad TADR = Ax \quad (\text{eq. 2})$$

148

149 Here *x* is an empirical parameter ( $\text{m s}^{-1}$ ), that describes the appropriate compositional flow parameters  
150 ( $\rho$ ,  $C_p$ ) as well as thermal insulation ( $T_e$ ) and cooling ( $T_0-T_{stop}$ ) conditions (cf. [Harris and Baloga](#)  
151 [2009](#)). In this formulation the area of the active flow area, *A* ( $\text{m}^2$ ) is also dependent on the insulation  
152 condition expressed by  $T_e$ , and is directly retrieved from the pixel integrated spectral radiance,  $R_\lambda$  ( $\text{W}$   
153  $\text{m}^{-2} \text{sr}^{-1} \mu\text{m}^{-1}$ ), according to:

154

$$155 \quad A = \sum_{i=1}^{npix} \frac{R_\lambda - L_\lambda(T_{bk})}{L_\lambda(T_e) - L_\lambda(T_{bk})} A_{pixel} \quad (\text{eq. 3})$$

156

157 where  $T_{bk}$  is the background temperature (K),  $L_\lambda$  is the Plank function for wavelength  $\lambda$  ( $\text{W m}^{-2} \text{sr}^{-1}$   
158  $\mu\text{m}^{-1}$ ), and  $A_{pixel}$  is pixel area ( $1 \text{ km}^2$  for MODIS). By assuming two end-member radiating  
159 temperatures ( $T_e$ ) for the hot and cold models (for example  $500^\circ\text{C}$  and  $100^\circ\text{C}$  for the channel- and  
160 tube-fed flow type, respectively), the equation 3 allows the user to calculate a range of plausible active  
161 flow areas, responsible for the observed radiance ([Harris et al., 2007](#)).

162 As stressed by [Harris and Baloga \(2009\)](#), the values for *x* have to be set on a case-by-case, thus leaving  
163 a wide arbitrariness to the user that may adjust all the unknowns in equation (1) to achieve a best-fit  
164 with available and independent field data. The TIR (thermal infrared) bands are generally used in this  
165 approach under the assumption that the surface area of high temperature cracks is small and provides  
166 a negligible contribution to the pixel integrated radiance at  $10 \mu\text{m}$  to  $12 \mu\text{m}$  ([Harris and Baloga 2009](#)).

167 This approach (equations 2 and 3) was the one used by [Bonny et al., \(2018\)](#) to estimate the volume  
168 of lava erupted during the 2014-2015 eruption at Holuhraun by using MODIS TIR data.

169

170 The method of [Coppola et al., 2013](#), does not hold with the calculation of active flow areas, but is  
171 based on the empirical relationship that directly links the *TADR* with the Volcanic Radiant Power  
172 (*VRP*) calculated via the MIR method ([Wooster et al., 2003](#)). The MIR-derived *VRP* is a measurement  
173 of the heat flux radiated almost exclusively by the portions of lava flows having effective temperature  
174 ( $T_e$ ) above 600 K, and is calculated as:

175

$$176 \quad VRP = 18.9 \cdot A_{\text{pixel}} \cdot \sum_{i=1}^{npix} (R_{MIR,alert} - R_{MIR,bk})_i \quad (\text{eq. 4})$$

177

178 where  $R_{MIR,alert}$  is the pixel integrated MIR radiance of the  $i^{\text{th}}$  alerted pixel,  $R_{MIR,bk}$  is the MIR radiance  
179 of the background,  $A_{\text{pixel}}$  is the pixel size (1 km<sup>2</sup> for the resampled MODIS pixels), and 18.9 is a  
180 constant of proportionality (see [Wooster et al., 2003](#)). The *TADR* is then calculated by using a single  
181 coefficient called radiant density ( $c_{\text{rad}}$  in J m<sup>-3</sup>):

182

$$183 \quad TADR = \frac{VRP}{c_{\text{rad}}} \quad (\text{eq. 5})$$

184

185 that describes the relationship between volumetric and radiant flux appropriate for the observed  
186 eruption ([Coppola et al., 2013](#)). By analyzing a large compositional spectrum of recent lava flows,  
187 [Coppola et al., \(2013\)](#) proposed an empirical method to calculate the  $c_{\text{rad}}$ , based on the silica content  
188 of the erupted lavas:

189

$$190 \quad c_{\text{rad}} = 6.45 \times 10^{25} \times (X_{\text{SiO}_2})^{-10.4} \quad (\text{eq. 6})$$

191 where  $X_{SiO_2}$  is the silica content of the erupted lavas (wt%).  
192 This method allows to take into account the strong effects that the bulk rheology has on the spreading  
193 and cooling processes of active lavas, and, according to the authors, permit to estimates  $TADR$  with  
194 an uncertainty of  $\pm 50\%$  (Coppola et al., 2013). Most importantly, it allows to calculate the appropriate  
195 radiant density, once the first chemical analysis of the erupted lavas become available (Coppola et  
196 al., 2017). Since the MIROVA system provides automatically the  $VRP$  (Coppola et al., 2016), the  
197 radiant density approach (equations 5 and 6) was the one used by Coppola et al., 2017 to estimate  
198  $TADR$  and erupted lava volume during the Holuhraun eruption.

199  
200 Although the two methods derive from the original heat balance approach, valid for cooling-limited  
201 lava flows (eq. 1), it is important to remark that they do not necessarily yield exactly the same results  
202 (cf. Bonny et al., 2018, Coppola et al., 2017). This is because the wavelengths used by the two  
203 methods are different ( $R_{TIR}$  and  $R_{MIR}$ , respectively) but also because of the arbitrariness of the input  
204 coefficients, as  $x$  for the Harris' method and  $c_{rad}$  for the Coppola's method. Nevertheless, both the  
205 methods provide an upper and lower boundary estimates of  $TADR$  that are *linearly* related to the  
206 pixel-integrated spectral radiances (cf. eq. 1 to 5). It follows that whatever the method used, a constant  
207  $TADR$  would be translated into a constant radiance detected by space.

208 This point was challenged by recent laboratory experiments and physical modelling of cooling  
209 viscous gravity currents (Garel et al., 2012, 2014, 2015) according to which for a given magma  
210 discharge rate the heat radiated by the flow surface reaches a steady value only after a transient time.  
211 According to the cooling-limited flow model (eq. 1), this transient time would correspond to the time  
212 required for the lava flow front to reach its maximum length ( $L$ ) and to cool to a halt ( $T_{front} = T_{stop}$ ).  
213 Hence, during rapid changes of effusion rates the thermal signal would be "buffered" in time, because  
214 it takes time for the higher flow rate to propagate downstream and cause perceptible increases in flow  
215 area (Harris and Baloga 2009). The transient time thus reflect the dynamic response of the thermal  
216 structure toward the appropriate cooling-limited conditions expressed by the new  $TADR$  vs.  $A$

217 relationship (i.e. new steady-state condition). [Tarquini \(2017\)](#) also suggests that this transient time is  
218 typical of non-equilibrium steady-state systems, and is related to a structural relaxation time that  
219 operate particularly on long-lived lava flows. In this non-equilibrium framework, the active lava flow  
220 units represent “dissipative structures” that promote significant fluctuations in the radiative power,  
221 even in the case of a constant supply. Hence, the radiant flux would be modulated by a pulsating  
222 emplacement dynamic, associated to the occurrence of flow diversions that resets the system further  
223 from its maximum extension (cf. [Tarquini 2017](#)).

224 Other open questions remain challenging, especially for operational use of the thermal proxy during  
225 effusive crisis. For example, based on its theoretical model, [Garel et al. \(2012\)](#) suggests that when  
226 lava tubes form, the surface thermal signal will not reflect the flow dynamics, because the low crust  
227 temperatures do not reflect a potentially high flow rate of hot lava underneath. According to the  
228 authors, this would pose a serious problem, since many lava flows exhibit evolving emplacement  
229 styles throughout the eruption, often characterized by increasing insulation conditions and gradual  
230 formation of lava tubes. Similarly, it is still unclear how to determine whether an eruption has ceased  
231 based on thermal data, or whether the lava stored underneath a cooled crust can potentially emerge  
232 suddenly and spread rapidly ([Garel et al., 2015](#)). In these terms the 2014-2015 eruption at Holuhraun  
233 represents a key-case since allowed us to address all these points over the largest effusive eruptions  
234 occurred in the past three centuries.

235

### 236 **3. Methods: Analysis of MODIS-MIR data**

#### 237 ***3.1 The MIROVA system***

238 MIROVA (Middle Infrared Observation of Volcanic Activity) is an automated global hot spot  
239 detection system ([www.mirovaweb.it](http://www.mirovaweb.it)) based on near-real time processing of Moderate Resolution  
240 Imaging Spectroradiometer (MODIS) infrared data ([Coppola et al. 2016](#)). The system completes  
241 automatic detection and location of thermal anomalies, and provides a quantification of the Volcanic

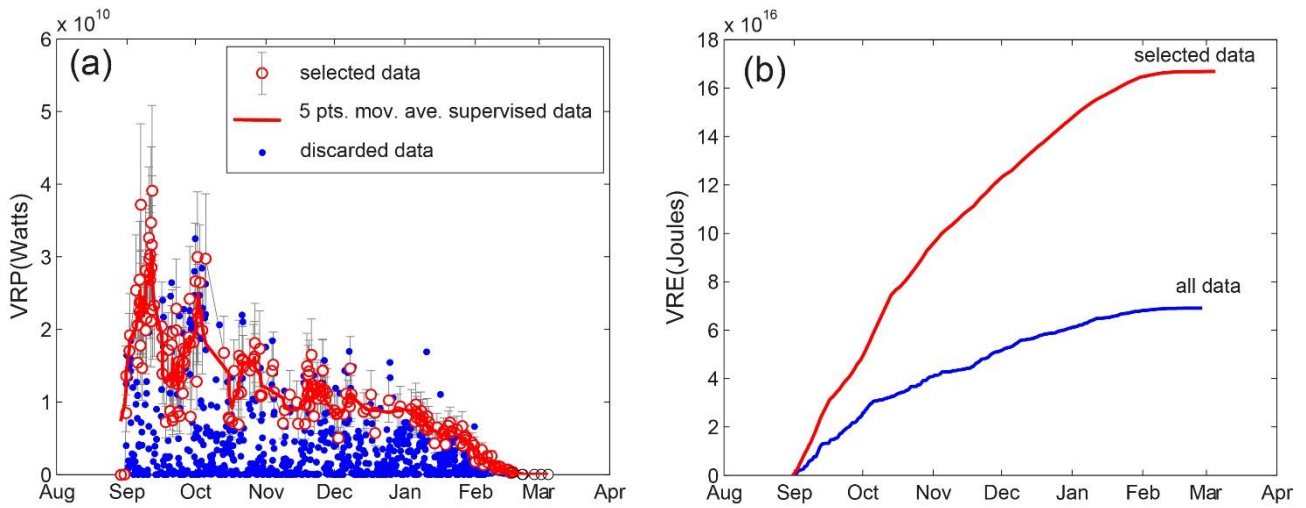
242 Radiative Power (*VRP*), within 1 to 4 hours of each satellite overpass. This is achieved through a  
243 hybrid algorithm (fully described in Coppola et al., 2016) based on MIR radiance data ( $\sim 4 \mu\text{m}$ )  
244 recorded at 1-km spatial resolution, as shown in Fig. 1b. Two MODIS instruments (carried on two  
245 NASA's satellites: Terra and Aqua) deliver approximately 4 images per day for every target volcano  
246 located at equatorial latitudes. However, due to the polar, sun-synchronous orbit, the two satellites  
247 increase their sampling time at high latitudes, providing, at least 6 to 10 overpasses per day over  
248 Iceland. An example of thermal images elaborated by the MIROVA system during the Holuhraun  
249 eruption is given in Fig. 1b.

250

### 251 ***3.2 Volcanic radiative power and energy of the 2014-2015 eruption at Holuhraun***

252 Between August 29<sup>th</sup>, 2014 and March 4<sup>th</sup>, 2015, MIROVA detected hotspots in 1105 images over a  
253 total of 1623 MODIS overpasses above Iceland ( $\sim 68.1\%$ ). The volcanic radiative power (*VRP*) ranged  
254 from  $\sim 39.1$  GW, during the initial stage of the effusion, to less than 10 MW just before the end of the  
255 eruption (Figure 2a). During the course of the eruption, we visually inspected all the acquired scenes  
256 and we identified a large number of images acquired in cloudy conditions, and/or under poor  
257 geometrical conditions that strongly deformed and affected the thermal anomaly at ground level.  
258 These images were discarded from further analysis (blue circles in Fig. 2a) so that a supervised dataset  
259 of only 206 high-quality images ( $\sim 12.7\%$  of the total MODIS overpasses) was used to provide a  
260 robust quantification of *VRP* produced by the eruption (red circles in Fig. 2a). As a whole we  
261 estimated that the Holuhraun eruption radiated approximately  $1.6 \times 10^{17}$  J into the atmosphere (red  
262 curve in Fig. 2b), with a time-averaged radiant flux of about 10.5 GW.

263



264

265

266

267

268

269

270

271

### 272 **3.3 Time-averaged discharge rates and volume calculation**

273

274

275

276

277

278

279

280

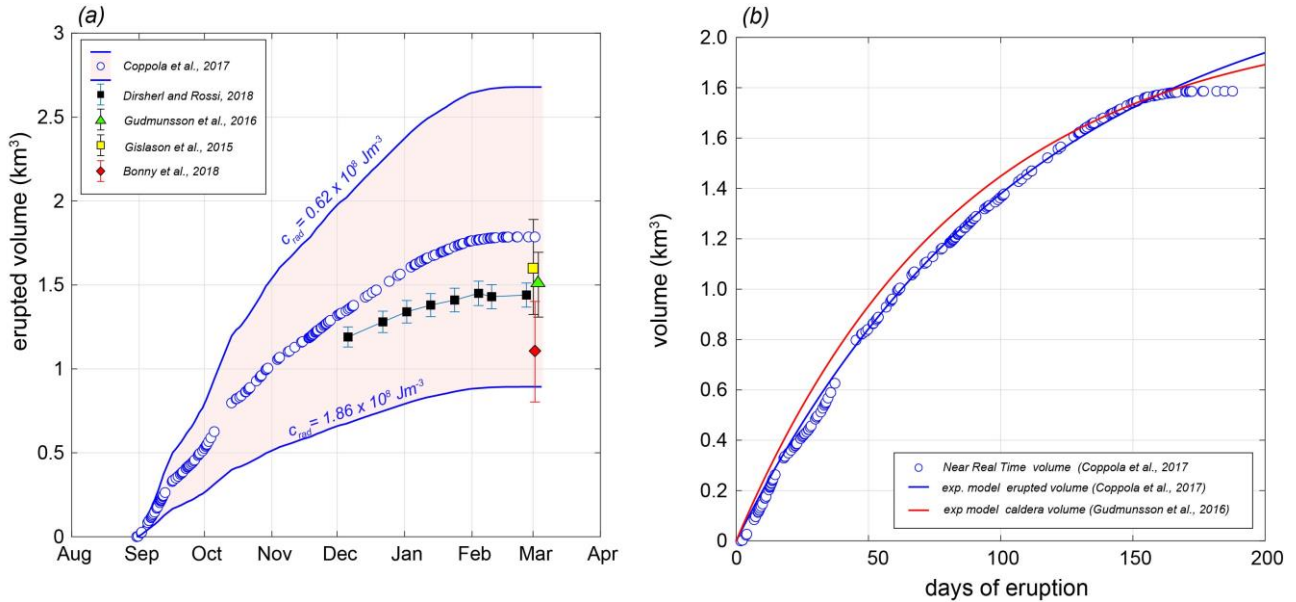
281

282

**Figure 2.** (a) Timeseries of *VRP* retrieved from MODIS-MIROVA system during the 2014-2015 eruption at Holuhraun. Blue circles represent data discarded because of cloudy conditions or poor viewing geometry. The data selected for *VPR* calculation are the white circles. The red line is a 5-points-moving average of *VRP*. A *VRP* below 10 MW coincides with the end of the eruption. (b) Volcanic Radiative Energy (*VRE*) calculated by trapezoidal integration of selected data only (red curve) or all the data (blue curve). Note the strong influence of data selection on the final total energy. Approximately  $1.6 \times 10^{17}$  J were radiated into the atmosphere (red curve), with a mean radiant flux of about 10.5 GW.

During the course of the eruption, we calculated *TADRs* and erupted lava volumes by using the radiant density approach described above (eq. 5 and 6). The preliminary chemical analysis of Holuhraun lavas ( $\text{SiO}_2 = 50.5$  wt%), provided in early September 2014 by the University of Iceland ([http://earthice.hi.is/bardarbunga\\_2014](http://earthice.hi.is/bardarbunga_2014)), were used to calculate (eq. 6) a radiant density comprised between  $0.62 \times 10^8$  and  $1.86 \times 10^8$   $\text{J m}^{-3}$ . These two values allowed us to provide an upper and lower boundary limits for lava volume calculation, with the mean value being the most likely (Fig. 3a). Given a final *VRE* equal to  $1.64 \times 10^{17}$  J (Fig. 2b), this method provided a first, timely assessment of the erupted lava volume equal to  $1.75 \pm 0.88$   $\text{km}^3$  (Fig. 3a). This was in good agreement with the flow volume estimated a-posteriori (  $1.4 - 1.6$   $\text{km}^3$ ) by using independent datasets (Gislason et al. 2015, Gudmundsson et al., 2016, Dirshel and Rossi, 2018; Bonny et al., 2018). The inferred satellite-

283 derived *TADR* and erupted volumes were updated continuously and delivered via emails to the teams  
 284 of the IMO and University of Iceland in charge of the monitoring.  
 285



286  
 287 **Figure 3.** (a) Lava volumes measured during the 2014-2015 eruption at Holuhraun. The colored field envelop the upper  
 288 and lower boundary limits calculated using the radiant density approach (eqs. 5 and 6). Best-estimate volume calculation  
 289 (blue circles), and relative uncertainty ( $\pm 50\%$ ) were provided in near real time to IMO and University of Iceland.  
 290 Independent measurements of final lava flow volumes given by several authors are also shown. (b) Comparison between  
 291 lava field volume measured by MODIS (blue circles) and exponential models of erupted lava volume (Coppola et al.,  
 292 2017) and caldera volume (Gudmunsson et al., 2016). The good correlation indicates a strong link between to the gravity-  
 293 driven collapse of Bárðarbunga caldera and the gradual decrease of magma-static pressure driving the effusive eruption  
 294 at the vent (cf. Gudmunsson et al., 2016, Coppola et al., 2017, Dirsheri and Rossi., 2018).

295  
 296

#### 297 **4. Eruptive trend derived from satellite thermal data**

298 One of the most significant feature of this eruption was the overall exponential trend of the satellite-  
 299 derived cumulative volume (Fig. 3b). As outlined by recent studies, this trend mirrors almost perfectly  
 300 the slow subsidence of the Bárðarbunga caldera floor (Fig. 3b) and suggests a strong connection  
 301 between source caldera/reservoir dynamic, and the eruptive dynamics 45 km distant (Gudmundsson

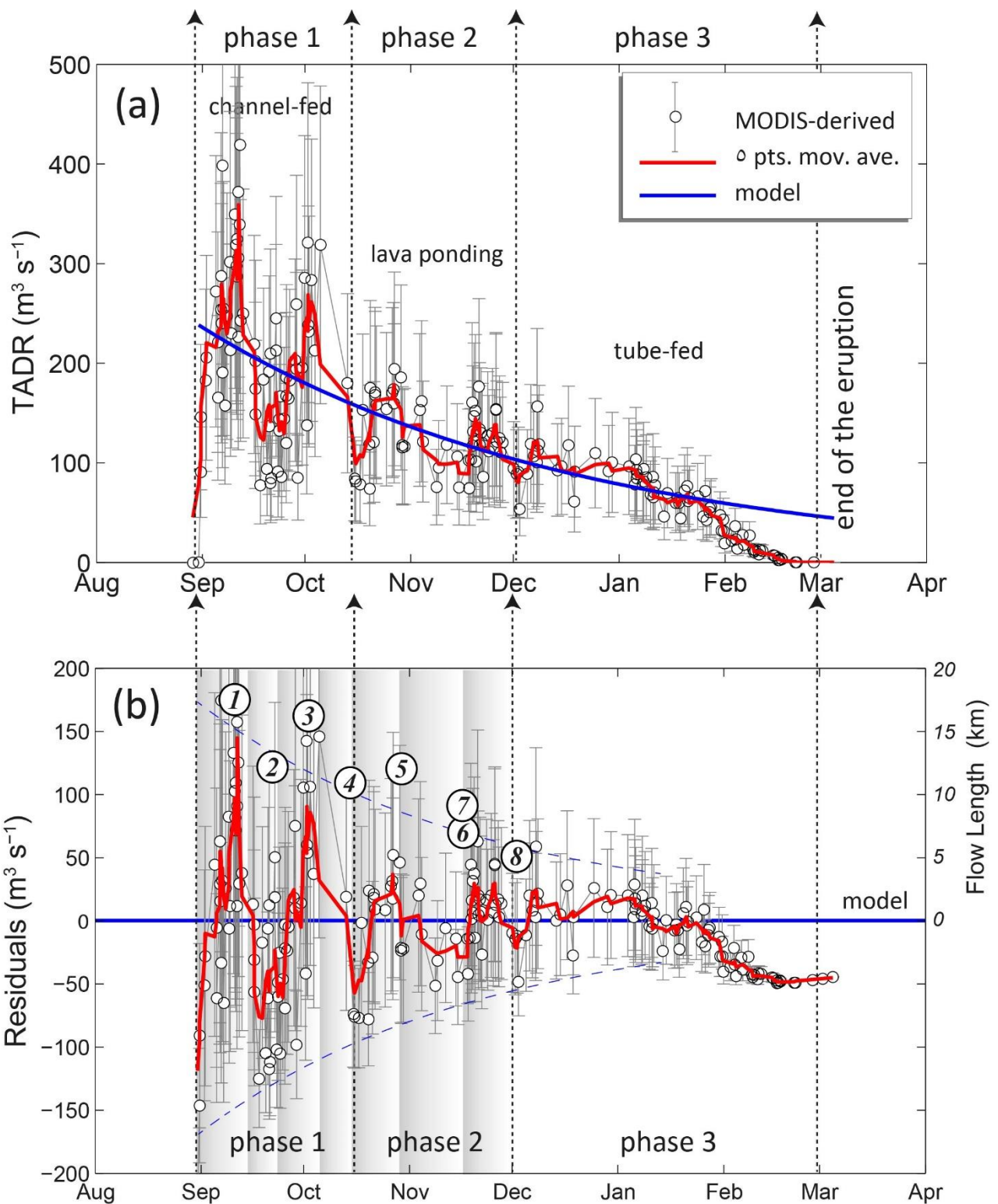
302 [et al., 2016](#); [Coppola et al., 2017](#)). According to these works, the exponential decay of effusion rates  
303 was driven by a decrease of magma-static pressure, associated to the shrinking of the magma chamber  
304 and the gravity-driven collapse of Bárðarbunga caldera. In this scenario, the instantaneous effusion  
305 rate at the vent follows a perfectly exponential curve (blue line in Fig 4a) that has been used as a  
306 benchmark for our MODIS-derived *TADRs*' (red line in Fig 4a). Hence, the residuals between the  
307 two rates (observed - modeled; Fig. 4b) enhance temporary variations of the source process, or  
308 instabilities of the thermal proxy due to lava flow emplacement dynamic. In the following section,  
309 we discuss the effusive trend in the light of the evolving emplacement style observed in the Holuhraun  
310 lava field.

311 According to [Pedersen et al. \(2017\)](#) the Holuhraun eruption can be subdivided in three main phases,  
312 characterized by evolving lava transport processes.

313 The phase 1 (*31 August – 12 October 2014*) was characterized by lava transport confined to *open*  
314 *channels* that led the formation of four consecutive lava flows emplaced side by side (no. 1–4 in Fig  
315 4b). During this phase the discharge rates measured on the field were comprised between 350 and  
316  $100 \text{ m}^3 \text{ s}^{-1}$  ([Pedersen et al., 2017](#)), in good agreement with satellite-derived values. The four flow  
317 units reached distances of 16.9, 11.8, 16.3 and 11.0 km, respectively (Fig. 4a), and covered a total  
318 area of  $58.31 \text{ km}^2$  ([Pedersen et al., 2017](#)). Given a flow field volume of  $0.78 \text{ km}^3$  estimated on October  
319 12 (Fig. 3b), the mean flow thickness characterizing the Phase 1 was 13.4 m, consistent with the  
320 thickness of each single flow units observed on the field ([Pedersen et al., 2017](#)). During this period  
321 our *TADRs* measurements show the greatest oscillations around the modelled value (up to  $\pm 60\%$ ),  
322 resulting in sharp variations exactly in correspondence of the activations of the distinct flow units  
323 (Fig 4b).

324





325

326 **Figure 4.** (a) *TADR* derived from MIROVA data (white circles) by using the radiant density approach (eqs. 5 and 6). The  
 327 blue line represents the best-fit exponential model (Coppola et al., 2017) hereby considered the real effusion rate at the  
 328 vent. (b) Residuals flow rates (left axis) obtained by subtracting the model from the observations (i.e. MODIS-derived  
 329 *TADR* minus modelled effusion rates). Note how the residuals oscillate around the model showing a decreasing amplitude  
 330 through time. The timing and amplitude of the residual pulses are coherent with the occurrence and maximum length of

331 the main channel-fed flow units numbered from 1 to 8 (data from Pedersen et al., 2017). The three phase of the eruption  
332 described by Pedersen et al., 2017 are also shown.

333

334 The phase 2 (13 October – 30 November 2014) had lower effusion rates ( $150 - 100 \text{ m}^3 \text{ s}^{-1}$ ) and was  
335 characterized by the formation of a  $< 1 \text{ km}^2$  lava pond, that acted as a distributor of subsequent lava  
336 flows (i.e. flows no. 5–8; Pedersen et al., 2017). These flow units reached gradually shorter distances  
337 (11.7, 8.4, 7.1, 5.4 km, respectively) and were accompanied by satellite-derived TADRs showing  
338 decreasing oscillation amplitudes (Fig. 4b). Towards the end of this phase the occurrence of *inflation*  
339 *plateaus* provided the first evidences of a growing lava tube system, with satellite-derived TADRs  
340 becoming more stable (Fig. 5b). About  $0.52 \text{ km}^3$ , of lava was erupted during this phase (Fig. 3a)  
341 producing a net increment of the flow field area of  $18.7 \text{ km}^2$  (Pedersen et al., 2017). By the end of  
342 November the flow field reached an average thickness of 16.9 m.

343 During the third phase (1 December 2014 – 27 February 2015) the lava transport was mainly confined  
344 to *lava tubes* which fed several breakouts and inflation plateaus along the initial flow units no. 1 and  
345 2 (Pedersen et al., 2017). More than  $19 \text{ km}^2$  of the flow field was resurfaced, with discharge rates  
346 much more steady ( $\pm 20\%$ ) and typically lower than  $100 \text{ m}^3 \text{ s}^{-1}$ . A sharp reduction of TADR was  
347 recorded since 27 January 2015 and precluded the end of the eruption occurred one month later, on the  
348 27 February 2015 (Fig.4). This reduction was interpreted by Coppola et al., (2017) as due to the  
349 gradual closure of the magma path once the overpressure inside the dike had dropped below a critical  
350 value. The lava tube system distributed about  $0.4 \text{ km}^3$  during this phase, with the lava field reaching  
351 a final extension of  $85.4 \text{ km}^2$ . The inflation and resurfacing processes that operated through the tube  
352 system led the average flow thickness to increase up to 20.2 m.

353

354 The emplacement of the major lava flows (phases 1 and 2) is outlined by the occurrence of apparent  
355 *TADR's* “pulses” (Fig. 4a) oscillating around the modelled value for effusion rate (Fig. 4b). Pulsating  
356 effusive activity has been recognized at several basaltic volcanoes and may results from different

357 processes such as pulsed magma supply, repeated accumulation and collapse of a foam layer at the  
358 reservoir roof, or by processes of magma mixing occurring within the magma chamber (e.g., [Harris](#)  
359 [and Neri 2002](#), [Lautze et al., 2004](#)). However, in the case of Holuhraun eruption, the link between the  
360 effusive trend and the collapse of the caldera (Fig. 3b) claims for a simple, gravity-driven dynamic  
361 ([Gudmundsson et al., 2016](#); [Coppola et al., 2017](#)) that would exclude, or minimize, the occurrence of  
362 above mentioned processes. Hence, the *TADR*'s pattern overprinted to the exponential trend is likely  
363 related to the emplacement dynamic occurred during the course of the eruption, and especially during  
364 the phases 1 and 2. Laboratory experiments ([Garel et al., 2012, 2014](#)) and theoretical treatments  
365 ([Tarquini 2017](#)), demonstrated that a constant effusion rate can actually produce pulses of the  
366 radiative power (Fig. 4b) that reflect the non-equilibrium steady-state growth of compound lava flow  
367 fields. According to [Tarquini \(2017\)](#) each flow unit will advance until the thermal equilibrium will  
368 be reached and the flow front stop. Hence, the system is resettled to give origin to a new flow unit.  
369 This seems to be exactly the dynamic occurred during the emplacement of the Holuhraun lava field,  
370 in which each apparent *TADR*'s pulse correlates with a phase of lengthening of a distinct flow unit.  
371 Notably, the amplitude of the pulses decreased with time as the overall effusion rate declined, the  
372 maximum length attained by the flow units reduced, and the emplacement style evolved from  
373 channel- to tube-fed (Fig. 4b).

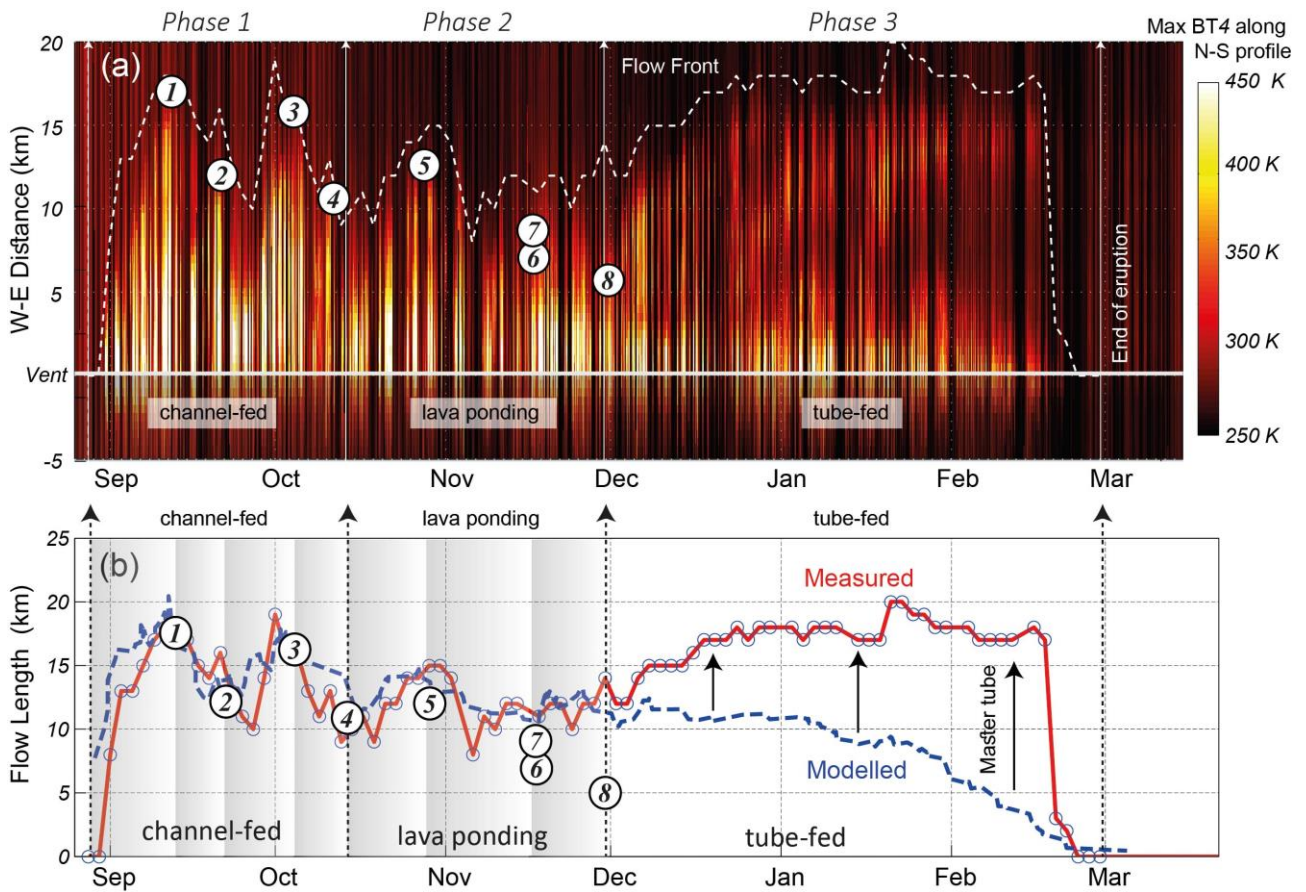
374

## 375 **5. Evolving emplacement style, evolving thermal structure**

376 In this section, we illustrate how the evolving emplacement style and the channel- to tube-fed  
377 transition affected the surface thermal structure of the Holuhraun's lava field. In particular, we used  
378 the temperature profiles (as the one shown in Fig. 1c) obtained from the MODIS image, in order to  
379 track the position of the active flow fronts and all the hot lava surfaces emerging along the principal  
380 flow path (from West to East). By stacking together all the W-E profiles the presence of active lavas  
381 (i.e. the vent(s), open-channel(s), breakout(s), flow front(s), etc.) appears as high-temperature features

382 (pixels), whose intensity, contiguity and extension can be easily visualized as shown in Fig. 5a. We  
383 assumed that the position of the flow front is represented by the easternmost pixel having a brightness  
384 temperature (BT4) of 50°C higher than the background (white dashed line in Fig. 5a). Hence, the  
385 distance between this pixel and the one located over the active vent (Fig. 1b), provides a measurement  
386 of the active flow length at each satellite overpass (red line in Fig. 5b). Lava flow lengths measured  
387 on the field during the phases 1 and 2 (Flows no. 1 to 8) are also plotted for comparison (Fig. 5b).

388 This analysis indicates that during the phases 1 and 2, the active flow fronts were thermally connected  
389 to the vents, through a high-radiating feature representing the open channels. On the other hand, since  
390 December 2014 the reduction of lava discharge rate caused a marked shortening of the open channels,  
391 although the lava field was still characterized by the presence of active lavas at the distal front(s).  
392 Notably, between the two hot, active zones (i.e. open channels and flow front) there low-temperature  
393 zone corresponding to crusted and cooling lava surfaces (Fig. 5a). This is a clear thermal evidence  
394 that since the beginning of the phase 3 the transport of lava occurred along a master tube system and  
395 that the emplacement style started to be *tube-fed* dominated.



396

397 **Figure 5.** (a) Evolution of the along-path thermal structure of the Holuhraun lava flow. This plot is obtained by stacking  
 398 together all the thermal profiles (max BT4 along each N-S line) as those illustrated in Fig. 1c. The white dashed line  
 399 indicate the position of the active flow front (see the text for details); (b) Comparison between measured (red dashed line)  
 400 and modelled (blue line) flow length. The Calvari & Pinkerton's model (eq. 7) assumes emplacement style dominated by  
 401 *channel-fed*, cooling limited conditions. The discrepancy between measured and modelled flow distance after December  
 402 2014 outline the increasing efficiency of *tube-fed* emplacement style in transporting the lava to the flow front.

403

404 As a pure theoretical exercise, the flow extension measured by using the temperature profiles has  
 405 been compared (Fig. 5b) with the maximum distance ( $L_{max}$ ) predicted by one of the simplest empirical  
 406 model developed for single, cooling-limited, channel-fed lava flow (cf. Walker 1973; Harris and  
 407 Rowland, 2009). In particular, we used the Calvari and Pinkerton's equation (1998) that takes into  
 408 account exclusively the *TADR*s measurements for the estimation of flow length:

409

410

$$L_{max} = 10^{3.11} \times (TADR)^{0.47} \quad (\text{eq.7})$$

411 The coefficients of equation 7 were empirically determined by regression analysis of single channel-  
412 fed Etnean lava flows lasting 1 to 12 days, a duration very similar to the single flow units observed  
413 at Holuhraun. This model does not require any knowledge of several others parameters (i.e.  
414 underlying slope, lava temperature, viscosity, velocity, channel width, channel depth, etc...) that are  
415 necessary to predict flow length using other approaches (see [Harris and Rowland 2009](#) for a review),  
416 but that are difficult, if not impossible to be constrained for each flow unit. However, despite its  
417 simplicity, this empirical model of Calvari and Pinkerton 1998 allows to calculate the maximum  
418 length of the Holuhraun's lava flow, and to see the effects of an emplacement style persistently  
419 dominated by channel-fed, cooling-limited conditions (blue line in Fig. 5b).

420 During the phases 1 and 2, there is an excellent correlation between the measured and the modelled  
421 flow lengths, both in terms of absolute values and pattern (Fig. 5b). This corroborate the fact that  
422 during this period the emplacement style was effectively those for which eq.7 was proposed to  
423 describe, that is single, channel-fed flows. Differently, since December 2014, there is a growing  
424 discrepancy between the measured and modelled flow length (Fig. 5b), exactly in correspondence of  
425 the formation of a master lava tube, as observed in the field ([Pedersen et al., 2017](#)).

426 From this picture, it is clear that the lower discharge rates characterizing the Phase 3, did not affect  
427 the maximum extent of the lava flow, still reaching a distance of more than 15 km, just before the end  
428 of the eruption (Fig. 5b). By paraphrasing [Harris and Rowland, \(2009\)](#) “the transition from poorly  
429 insulated (*channel-fed*) to well insulated (*tube-fed*) regimes increases the length that a lava flow can  
430 extend for a given *TADR*”.

431 Notably, we may calculate the radiant density ( $c_{rad} = VRE/Vol$ ) typical of the tube-fed flow field, by  
432 dividing the thermal energy measured during the Phase 3 ( $VRE = \sim 0.4 \times 10^{17}$  J; Fig. 2b) by the  
433 volume lava erupted in the same time window, derived from Tandem-X measurements ( $Vol = 2.6 \times$   
434  $10^8$  m<sup>3</sup>; Fig. 3a; [Dirscherl and Rossi 2018](#)). The resulting radiant density ( $c_{rad} = \sim 1.5 \times 10^8$  J m<sup>-3</sup>) is  
435 only slightly higher than the radiant density calculated in the same way for the bulk channel-fed flow  
436 field emplaced during phases 1 and 2 ( $c_{rad} = \sim 1.1 \times 10^8$  J m<sup>-3</sup>). This suggests that the variation of the

437 emplacement style produces an uncertainty in the *TADR*s measurement that does not exceed 30%,  
438 when provided in near real time. In other words, our results point out that, the formation of a lava  
439 tube does not affect substantially the amount of “active” lava radiating to the atmosphere, but simply  
440 “made this lava to be transported further from the vent”. The lava tube thus act as a simple extension  
441 of the volcanic conduit, by displacing the vent downstream, likely along the main axis of the  
442 previously formed flow units. The recognition of this behavior in near real time allow to update the  
443 vent location and has been proved to be a necessary improvement to correct estimation of the lava  
444 flow path and the effective runout distance (Harris et al., 2018, this issue).

445

#### 446 ***6. Operational use of MIROVA system during the effusive crisis***

447 By the end of November 2014, MIROVA started to be part of the monitoring system operative at the  
448 Icelandic Meteorological Office (IMO) with the coverage of nine active volcanic systems. IMO is the  
449 main institution in Iceland in charge of monitoring natural hazards and issuing forecast and warnings  
450 in case of impending or on-going eruptions. It operates a multi-sensors network that includes  
451 seismometers, GPS and gas sensors for the geophysical monitoring. During the Holuhraun eruption,  
452 gas monitoring activity was improved and new instrumentations were deployed and maintained at the  
453 eruption site for the entire duration of the event (Pfeffer et al. 2017). The MIROVA system showed  
454 its strength and reliability in a period of the year when, in Iceland, the day light time is very short.  
455 Several of the instrumentations and products that could normally be used to monitor an eruption,  
456 started to fail or to give incomplete data sets due to harsh weather conditions and limited sunlight.  
457 MIROVA provided a robust and continuous data set on a daily basis which was used from November  
458 to March to follow the health and strength of the eruption, as well as the post-eruption phase.  
459 On the operative side this system is revealed to be an important monitoring tool for following the  
460 temporal evolution of the eruption and providing estimates of the erupted lava volume in near real  
461 time (Coppola et al., 2017). Extrapolation of the effusive trend during the ongoing eruption may in

462 fact be used to forecast total erupted lava volume, which in turn is fundamental to drive some lava  
463 flow modelling (i.e. [Tarquini et al., 2018](#)). Also, the recognition of emplacement style through the  
464 analysis of flow' surface thermal structure (i.e. channel- or tube-fed lava flows) can be used to update  
465 the position of active flow fronts, and to choose the appropriate modeling strategy, by tuning some  
466 appropriate parameters that govern lava flow simulation's codes (i.e. [Tarquini et al., 2018, this issue](#)).  
467 Most importantly the thermal data have proved to be very important for constraining the time of the  
468 eruption end. A drastic change of *TADR* was observed since the end of January 2015 becoming clear  
469 the second week of February 2015 (Fig. 4a). This change was interpreted by [Coppola et al. \(2017\)](#) as  
470 due to the gradual closure of the magma path (dike) and indicated the potential timing of the end of  
471 the eruption in quite a good advance, about one month before the declaration of ceased eruption.  
472 These data were discussed within the Scientific Board Management meetings that were held from the  
473 beginning of the eruption in collaboration with the Icelandic Civil Protection and the University of  
474 Iceland. The very low *TADR* detected on 26 February 2017 ( $0.2 \text{ m}^3 \text{ s}^{-1}$ ; Fig. 4a), supported the  
475 decision for a field crew to flight over the eruptive site on February 27 and declare that the eruption  
476 was over.

477 The thermal data were useful for providing a semi-quantitative indication of the strength of the gas  
478 source affecting the ground level concentration ([Simmons et al., 2017](#)). Due to its extension the lava  
479 field itself was a considerable source of volcanic gases. In addition, the gas released close to the  
480 surface was more easily trapped within the boundary layer and largely affected the concentration at  
481 ground. This fact suggested that the MIROVA detection and the *VRP* temporal variation could be  
482 correlated with the amount of gases released at the source. In this way the *VRP* data have been used  
483 by the forecasters at IMO to identify, in a qualitative way, when to expect an increase in the  $\text{SO}_2$   
484 values in areas located downwind the eruption site.

485

486



## 487 7. Conclusions

488 During the 2014-2015 Bárðarbunga-Holuhraun eruptive crisis, one of the main challenge for the  
489 volcanological community was to monitor the effusive process in a safely, timely and routinely  
490 manner. For the whole duration of the eruption, MIROVA provided a robust and continuous set of  
491 thermal data that were used to depict the effusive trend and to estimates the erupted lava volume  
492 although the changing emplacement conditions (from channel- to tube-fed flow) introduced  
493 uncertainties in the interpretation of the data.

494 The retrospective analysis of this eruption provides an exceptional opportunity to study the  
495 relationship between heat flux and *TADR* during the emplacement of a large compound lava field.  
496 We show that the overall trend of thermal emission was related to the combined effect of two over  
497 imposed patterns: (i) a main exponential decay of the effusion rate trend, governed by the source  
498 processes and (ii) a secondary pulsating pattern related to the emplacement dynamic of the flow field.  
499 We found that the magnitude and timing of these pulses were strictly related to the timing and length  
500 scales of discrete flow units characterizing open-channel lava transport. Conversely, the formation of  
501 lava tubes produces smaller instabilities and promotes lava to flow at greater distance in steady-state  
502 thermal conditions. This process is clearly visible from the evolution of the thermal structure depicted  
503 from the MODIS-MIROVA images and allow to track changes in the *lava transport mechanisms*  
504 operating during the eruption (Fig. 5a). The results presented here clearly indicate that the calculation  
505 of erupted lava volumes from the integration of satellite-derived *TADR* allow to smooth the short-  
506 term perturbation associated to the emplacement dynamic and provide a robust way to depict source  
507 eruptive trends. We thus regard the application of this methodology as a key-factor in volcano  
508 monitoring and satellite-data-driven response to an effusive crisis (Harris et al., 2018).

509

510

511

512 **Acknowledgments**

513 MIROVA is a collaborative project between the Universities of Turin and Florence (Italy) and is  
514 supported by the Centre for Volcanic Risk of the Italian Civil Protection Department. We  
515 acknowledge the LANCE-MODIS data system for providing MODIS Near Real Time products.

516

517 **References**

518 Bonny, E., T. Thordarson, R. Wright, A. Höskuldsson, I. Jónsdóttir (2018) The volume of lava  
519 erupted during the 2014 to 2015 eruption at Holuhraun, Iceland: A comparison between satellite  
520 and ground-based measurements, *J Geophys Res Solid Earth*, 123.  
521 <https://doi.org/10.1029/2017JB015008>.

522 Calvari, S. and H. Pinkerton (1998) Formation of lava tubes and extensive flow field during the 1991–  
523 1993 eruption of Mount Etna, *J. Geophys Res*, B103, 27291–27301.

524 Coppola, D., M. Laiolo, D. Piscopo and C. Cigolini (2013) Rheological control on the radiant density  
525 of active lava flows and domes, *J. Volcanol. Geotherm. Res.*, 249, 39–48.  
526 doi:10.1016/j.jvolgeores.2012.09.005.C.

527 Coppola, D., M. Laiolo, C. Cigolini, D. Delle Donne and M. Ripepe (2016) Enhanced volcanic hot-  
528 spot detection using MODIS IR data: Results from the MIROVA system, in Harris A. J. L. , T.  
529 De Groot, F. Garel and S. A. Carn (eds.) *Detecting, Modelling, and Responding to Effusive*  
530 *Eruptions*, Geological Society, London, Sp. Pub. 426, p. 181–205, doi:10.1144/SP426.5.

531 Coppola, D., M. Ripepe, M. Laiolo and C. Cigolini (2017) Modelling Satellite-derived magma  
532 discharge to explain caldera collapse, *Geology* 45(6), 523-526. doi:10.1130/G38866.1.

533 Crisp, J. and S. Baloga (1990) A method for estimating eruption rates of planetary lava flows, *Icarus*,  
534 85(2), 512-515.

535 Crisp, J. and S. Baloga (1990) A model for lava flows with two thermal components, *J. Geophys.*  
536 *Res.*, 95 (B2), 1255-1270.

537 Dirsherl, M. and C. Rossi (2018) Geomorphometric analysis of the 2014–2015 Bárðarbunga volcanic

538 eruption, Iceland, *Remote Sens. Environ.*, 204, 244-259.

539 Dragoni, M. and A. Tallarico (2009), Assumptions in the evaluation of lava effusion rates from heat  
540 radiation, *Geophys. Res. Lett.*, 36, L08302. doi:10.1029/2009GL037411.

541 Garel, F., E. Kaminski, S. Tait and A. Limare (2012) An experimental study of the surface thermal  
542 signature of hot subaerial isoviscous gravity currents: implications for thermal monitoring of  
543 lava flows and domes, *J. Geophys. Res.* 117:B02205. doi: 10.1029/2011JB008698.

544 Garel, F., E. Kaminski, S. Tait and A. Limare (2014) An analogue study of the influence of  
545 solidification on the advance and surface thermal signature of lava flows, *Earth Planet. Sci.*  
546 *Lett.*, 396, 46–55.

547 Garel, F., E. Kaminski, S. Tait and A. Limare (2015) A fluid dynamics perspective on the  
548 interpretation of the surface thermal signal of lava flows, , in Harris A. J. L. , T. De Groeve, F.  
549 Garel and S. A. Carn (eds.) *Detecting, Modelling, and Responding to Effusive Eruptions*,  
550 Geological Society, London, Sp. Pub. 426, 243-256. doi: 10.1144/SP426.6

551 Gíslason, S. R., G. Stefánsdóttir, M. A. Pfeffer, S. Barsotti, Th. Jóhannsson, I. Galeczka, E. Bali, O.  
552 Sigmarsson, A. Stefánsson, N. S. Keller, A. Sigurdsson, B. Bergsson, B. Galle, V. C. Jacobo,  
553 S. Arellano, A. Aiuppa, E. B. Jónasdóttir, E. S. Eiríksdóttir, S. Jakobsson, G. H. Guðfinnsson,  
554 S. A. Halldórsson, H. Gunnarsson, B. Haddadi, I. Jónsdóttir, Th. Thordarson, M. Riishuus, Th.  
555 Högnadóttir, T. Dürig, G. B. M. Pedersen, A. Höskuldsson and M. T. Gudmundsson (2015)  
556 Environmental pressure from the 2014–15 eruption of Bárðarbunga volcano, Iceland,  
557 *Geochem. Persp. Lett.*, 1, 84-93.

558 Gudmundsson, A., N. Lecoeur, N. Mohajeri and T. Thordarson (2014) Dike emplacement at  
559 Bárðarbunga, Iceland, induces unusual stress changes, caldera deformation, and earthquakes,  
560 *Bull. Volcanol.*, 76, 869–875. doi:10.1007/s00445-014-0869-8.

561 Gudmundsson, M. T., K. Jónsdóttir, A. Hooper, E. P. Holohan, S. A. Halldórsson, B. G. Ófeigsson,  
562 S. Cesca, K. S. Vogfjörð, F. Sigmundsson, T. Högnadóttir, P. Einarsson, O. Sigmarsson, A. H.  
563 Jarosch, K. Jónasson, E. Magnússon, S. Hreinsdóttir, M. Bagnardi, M. M. Parks, V.

564 Hjörleifsdóttir, F. Pálsson, T. R. Walter, M. P. Schöpfer, S. Heimann, H. Reynolds, S. Dumont,  
565 E. Bali, G. H. Gudfinnsson, T. Dahm, M. J. Roberts, M. Hensch, J. M. Belart, K. Spaans, S.  
566 Jakobsson, G. B. Gudmundsson, H. M. Fridriksdóttir, V. Drouin, T. Dürig, G. Aðalgeirsdóttir,  
567 M. S. Riishuus, G. B. Pedersen, T. van Boeckel, B. Oddsson, M. A. Pfeffer, S. Barsotti, B.  
568 Bergsson, A. Donovan, M. R. Burton, A. Aiuppa (2016) Gradual caldera collapse at  
569 Bárðarbunga volcano, Iceland, regulated by lateral magma outflow, *Science*, 353.  
570 doi:10.1126/science.aaf8988.

571 Harris, A. J. L. and M. Neri (2002) Volumetric observations during paroxysmal eruptions at Mount  
572 Etna: Pressurized drainage of a shallow chamber or pulsed supply?, *J. Volcanol. Geotherm.*  
573 *Res.*, 116, 79–95, doi:10.1016/S0377-0273(02)00212-3.

574 Harris, A. J. L. and S. Baloga (2009) Lava discharge rates from satellite-measured heat flux, *Geophys.*  
575 *Res. Lett.*, 36, L19302. doi:10.1029/2009GL039717.

576 Harris, A. J. L. and S. K. Rowland (2009) Effusion rate controls on lava flow length and the role of  
577 heat loss; a review, in Thordarson, T., S. Self, G. Larsen, S. K. Rowland and A. Hoskuldsson  
578 (eds) *Studies in Volcanology: The Legacy of George Walker*. Geological Society, London Sp.  
579 *Pub. of IAVCEI*, 2, 33– 51.

580 Harris, A. J. L., S. Blake, D. A. Rothery, and N. F. Stevens (1997) A chronology of the 1991 to 1993  
581 Etna eruption using AVHRR data: Implications for real time thermal volcano monitoring, *J.*  
582 *Geophys. Res.*, 102(B4), 7985–8003, doi:10.1029/96JB03388.

583 Harris, A. J. L., J. Dehn, and S. Calvari (2007) Lava effusion rate definition and measurement: A  
584 review, *Bull. Volcanol.*, 70, 1–22. doi:10.1007/s00445-007-0120-y.

585 Harris, A. J. L., S. Carn, J. Dehn, C. Del Negro, G. Guðmundsson, B. Cordonnier, T. Barnie, S.  
586 Calvari, T. Catry, T. de Groot, D. Coppola, A. Davies, M. Favalli, E. Fujita, G. Ganci, F.  
587 Garel, J. Kauahikaua, K. Kelfoun, V. Lombardo, G. Macedonio, J. Pacheco, M. Patrick, N.  
588 Pergola, M. Ramsey, R. Rongo, K. Smith, S. Tarquini, T. Thordarson, N. Villeneuve, P.  
589 Webley, R. Wright and K. Zakzek (2016a) *Conclusion: Recommendations and findings of the*

590 RED SEED working group, in Harris A. J. L., T. De Groeve, F. Garel and S. A. Carn (eds.)  
591 Detecting, Modelling, and Responding to Effusive Eruptions, Geological Society, London, Sp.  
592 Pub. 426, p. 567-648. doi:10.1144/SP426.11.

593 Harris, A. J. L., T. De Groeve, S. Carn, F. Garel (2016b) Risk evaluation, detection and simulation  
594 during effusive eruption disasters, in Harris A. J. L., T. De Groeve, F. Garel and S. A. Carn  
595 (eds.) Detecting, Modelling, and Responding to Effusive Eruptions, Geological Society,  
596 London, Sp. Pub. 426, p. 1-22. doi:10.1144/SP426.29.

597 Harris, A. J. L., O.M. Chevrel, D. Coppola, M.S. Ramsey, A. Hrysiewicz, S. Thivet, N. Villeneuve,  
598 M. Favalli, A. Peltier, P. Kowalski, A Di Muro, J-L Froger, L. Gurioli (2018) Validation of  
599 an integrated satellite-data-driven response to an effusive crisis: 2 the April–May 2018 eruption  
600 of Piton de la Fournaise, Special Issue: MeMoVolc, Annals of Geophysics, (in press, this issue)

601 Lautze, N. C., A. J. L. Harris, J. E. Bailey, M. Ripepe, S. Calvari, J. Dehn, S. Rowland, and K. Evans-  
602 Jones (2004) Pulsed lava effusion at Mount Etna during 2001, J. Volcanol. Geotherm. Res.,  
603 137, 231–246. doi:10.1016/j.jvolgeores.2004.05.018

604 Pedersen, G. B. M., A. Höskuldsson, T. Dürig, T. Thordarson, I. Jónsdóttir, M. S. Riishuus, B. V.  
605 Óskarsson, S. Dumont, E. Magnusson, M. T. Gudmundsson, F. Sigmundsson, V. J. P. B.  
606 Drouin, C. Gallagher, R. Askew, J. Gudnason, W. M. Moreland, P. Nikkola, H. I. Reynolds, J.  
607 Schmith and the IES eruption team (2017). Lava field evolution and emplacement dynamics of  
608 the 2014–2015 basaltic fissure eruption at Holuhraun, Iceland, J. Volcanol. Geotherm. Res.,  
609 10.1016/j.jvolgeores.2017.02.027.

610 Pfeffer, M. A., B. Bergsson; S. Barsotti; G. Stefánsdóttir; B. Galle, S. Arellano, V. Conde, A.  
611 Donovan, E. Ilyinskaya, M. Burton, A. Aiuppa, R. C. W. Whitty, I. C. Simmons, Þ. Arason, E.  
612 B. Jónasdóttir, N. S. Keller, R. F. Yeo, H. Arngrímsson, Þ. Jóhannsson, M. K. Butwin, R. A.  
613 Askew, S. Dumont, S. von Löwis, Þ. Ingvarsson, A. La Spina, H. Thomas, F. Prata, F. Grassa,  
614 G. Giudice, A. Stefánsson, F. Marzano, M. Montopoli and L. Mereu (2017) Ground-Based  
615 Measurements of the 2014–2015 Holuhraun Volcanic Cloud (Iceland), Geosciences, 8, 29.

- 616 Pieri, D. and S. M. Baloga (1986) Eruption rate, area, and length relationships for some Hawaiian  
617 lava flows, *J. Volcanol. Geotherm. Res.*, 30 (1), 29-45.
- 618 Ramsey, M. and A. J. L. Harris (2013) Volcanology 2020: How will thermal remote sensing of  
619 volcanic surface activity evolve over the next decade? *J. Volcanol. Geotherm. Res.*, 249, 217-  
620 233.
- 621 Sigmundsson, F., A. Hooper, S. Hreinsdóttir, K. S. Vogfjörð, B. G. Ófeigsson, E. R. Heimisson, S.  
622 Dumont, M. Parks, K. Spaans, G. B. Gudmundsson, V. Drouin, T. Árnadóttir, K. Jónsdóttir, M.  
623 T. Gudmundsson, T. Högnadóttir, H. M. Fridriksdóttir, M. Hensch, P. Einarsson, E.  
624 Magnússon, S. Samsonov, B. Brandsdóttir, R. S. White, T. Ágústsdóttir, T. Greenfield, R. G.  
625 Green, A. R. Hjartardóttir, R. Pedersen, R. A. Bennett, H. Geirsson, P. C. La Femina, H.  
626 Björnsson, F. Pálsson, E. Sturkell, C. J. Bean, M. Möllhoff, A. K. Braiden and E. P. S. Eibl  
627 (2015) Segmented lateral dyke growth in a rifting event at Bárðarbunga volcanic system,  
628 Iceland, *Nature*, 517, 191–195.
- 629 Sigurðsson, H. and R. S. J. Sparks (1978) Rifting episode in North Iceland in 1874–1875 and the  
630 eruptions of Askja and Sveinagja, *Bull. Volcanol.*, 41, 149–167.
- 631 Simmons, I, M. A. Pfeffer, E. Calder, B. Galle, S. Arellano, D. Coppola and S. Barsotti (2017)  
632 Extended SO<sub>2</sub> outgassing from the 2014-2015 Holuhraun lava flow field, Iceland, *Bull.*  
633 *Volcanol.*, X. DOI: 10.1007/s00445-017-1160-6.
- 634 Tarquini, S. (2017) A review of mass and energy flow through a lava flow system: insights provided  
635 from a non-equilibrium perspective, *Bull. Volcanol.*, 79, 64. [https://doi.org/10.1007/s00445-](https://doi.org/10.1007/s00445-017-1145-5)  
636 [017-1145-5](https://doi.org/10.1007/s00445-017-1145-5).
- 637 Tarquini, S., M. de' Michieli Vitturi, E. Jensen, G. Pedersen, S. Barsotti, D. Coppola, M. A. Pfeffer  
638 (2018) Modeling lava flow propagation over a flat landscape by using MrLavaLoba: the case  
639 of the 2014–2015 eruption at Holuhraun, Iceland, Special Issue: MeMoVolc, *Annals of*  
640 *Geophysics*, 61. <https://doi.org/10.4401/ag-7812>.

641 Walker, G. P. L. (1973) Lengths of lava flows. *Philosophical Transactions of the Royal Society*,  
642 London, 274, 107–118.

643 Wooster, M. J., B. Zhukov and D. Oertel (2003) Fire radiative energy for quantitative study of  
644 biomass burning: derivation from the BIRD experimental satellite and comparison to MODIS  
645 fire products, *Remote Sens. Environ.*, 86, 83–107. [http://dx.doi.org/ 10.1016/S0034-](http://dx.doi.org/10.1016/S0034-4257(03)00070-1)  
646 [4257\(03\)00070-1](http://dx.doi.org/10.1016/S0034-4257(03)00070-1).

647 Wright, R., S. Blake, A. J. L. Harris, and D. Rothery (2001) A simple explanation for the space-  
648 based calculation of lava eruption rates, *Earth Planet. Sci. Lett.*, 192, 223 – 233.  
649 [doi:10.1016/S0012-821X\(01\)00443-5](https://doi.org/10.1016/S0012-821X(01)00443-5).

650